thermo

MDPI

Article

Steady-State Feasibility of a Phase Change Material-Based Defrosting System and Energy Storage Management Strategies

Adrian Chiriac, Horatiu Pop *, Valentin Apostol *, Claudia Ionita and Daniel Taban

Department of Engineering Thermodynamics, Engines, Thermal and Refrigeration Equipment, National University of Science and Technology POLITEHNICA Bucharest, Splaiul Independenței 313, 060042 Bucharest, Romania; gabriel.chiriac@upb.ro (A.C.); claudia.ionita@upb.ro (C.I.); daniel.taban@upb.ro (D.T.)

* Correspondence: horatiu.pop@upb.ro (H.P.); valentin.apostol@upb.ro (V.A.); Tel.: +40-744903488 (H.P.); +40-744570329 (V.A.)

Abstract

The present work proposes a phase change material-based defrosting system (PCM-DS) for vapor compression refrigeration systems (VCRSs). The primary objective is to determine the optimal PCM mass and refrigerant mass flow rate required to melt 1 kg of accumulated evaporator ice. A steady-state macroscopic thermodynamic model, governed by global energy balances and driven by experimental boundary conditions, evaluates the VCRS in both cooling and defrosting operating modes. The PCM-DS is not installed on the experimental setup. The latter is used to obtain experimental data to be used as inputs in the steady-state model. Among the three candidates investigated (OM42, OM46, OM48), OM42 was selected for minimizing system mass and volume constraints. Results demonstrate that integrating the PCM-DS induces only a 3% reduction in the theoretical coefficient of performance (COP) compared with a 5.6% reduction in the case of using the electric heater defrosting (EHD). The core innovation of this work involves proposing and evaluating three distinct energy storage management strategies: unique superheating, unique bypass, and intermittent bypass. The results show that the highest COP is obtained for unique superheating (2.93), followed by unique bypass (2.82) and intermittent bypass (2.81). The work conducted proves the theoretical feasibility of such PCM-DS.

Keywords: vapor compression; defrosting; phase change material; energy storage strategies

1. Introduction

Heating, Ventilation, Air Conditioning and Refrigeration (HVAC&R) systems operating on the vapor compression cycle are responsible for a significant share of direct and indirect greenhouse gas emissions. Although there are different values from one country to another, the energy consumption of these systems accounts for approximately 16% to 50% of the total energy used in buildings [1].

The operation of vapor compression refrigeration systems (VCRSs) also requires defrosting periods, which contribute to the overall energy consumption of these systems. Frost accumulation negatively affects the entire system by partially or completely obstructing the airflow, which can lead to a significant deterioration of heat transfer that would determine lower evaporating pressure, and lastly, a reduction in the performance of the refrigeration system [2].

In case of VCRSs, there are several types of defrost methods, namely: air defrost [3], electric heating defrost [4], hot gas defrost [5], reverse cycle defrost [6] and hot water

Check for updates

Academic Editor: Ignazio Blanco

Received: 8 April 2026
Revised: 29 May 2026
Accepted: 5 June 2026
Published: 11 June 2026

Copyright: © 2026 by the authors. Licensee MDPI, Basel, Switzerland. This article is an open access article distributed under the terms and conditions of the Creative Commons Attribution (CC BY) license.

defrost [7]. At the same time, methods for frost formation inhibition are available, such as coating [8], desiccant [9], ultrasound [10] or electric field [11]. While these conventional active and passive techniques are widely adopted in commercial applications, they inevitably introduce energy penalties such as consuming additional electrical power or interrupting the cooling cycle. As a consequence, these factors are significantly reducing the overall coefficient of performance (COP) of the VCRSs [12].

Recent studies have shown that the defrosting process in VCRSs can be optimized using phase change materials (PCMs) by means of thermal energy storage (TES) [13]. The broad applicability and high efficiency of PCMs in managing transient thermal loads have been extensively documented for various temperature ranges, including specific applications in refrigeration, building thermal management, and general latent heat storage [14]. This approach has received significantly less attention in the literature compared to the defrosting methods previously mentioned. From the authors' knowledge, most of the papers published on PCM-based defrost methods are conducted for heat pump applications.

The specific application of TES systems is to capture available energy and use it to extend product preservation time, as well as in other applications such as defrosting of evaporators in heat pumps and VCRSs [15]. In case of VCRSs, TES systems designed for the defrosting process can operate using the energy available between the compressor discharge and the condenser, during the condensing process or during the subcooling process [16].

Ref. [17] conducted an experimental study where the compressor of a refrigeration system was wrapped with PCM. Results showed that the energy used for defrosting was 27.9% lower compared to reverse cycle defrosting. Similarly, the energy available at the compressor discharge was employed for defrosting a domestic refrigerator in the study conducted by [18]. Defrosting time was reduced by 65–77% compared with electric heating defrost (EHD). The defrosting energy consumption decreased by 89–92%. Ref. [19] conducted an experimental study on a heat pump system using condensation-based TES. Results demonstrated that the defrosting time was reduced by nearly 40% compared to the conventional hot gas defrosting method.

Ref. [20] proposed a subcooling energy storage method for an air source heat pump using a heat exchanger integrated with a PCM. Results of their study show that the defrosting time was reduced by more than 30%, while the energy consumed during defrosting decreased by 13.9% compared with reverse cycle defrosting.

Previous research investigated the thermal behavior of PCM heat exchangers, focusing on the melting and solidification processes, heat transfer enhancement, and overall component design [21,22]. While these studies focus strictly on the component level, the thermodynamic integration of PCM units into the overall refrigeration system must also be evaluated. Such system-level integrations are essential for recovering waste heat and improving the energy efficiency of vapor compression cycles [23].

In this context, a research gap is the lack of comparative data regarding specific energy storage management strategies for PCM-DS integrated into VCRSs. Therefore, the present work proposes and analyzes, in steady-state conditions, a PCM-based defrosting system that utilizes the energy available during the desuperheating process. The innovation of this work consists of three main directions: (i) thermal energy storage defrosting method using phase change materials and the heat available after the compression process; (ii) the schematic of the defrosting system integrating a refrigerant to phase change material heat exchanger; and (iii) proposing and evaluating three distinct energy storage management strategies: unique superheating, unique bypass and intermittent bypass, the most suitable being the unique superheating strategy due to a lower VCRS schematic complexity and higher theoretical COP.

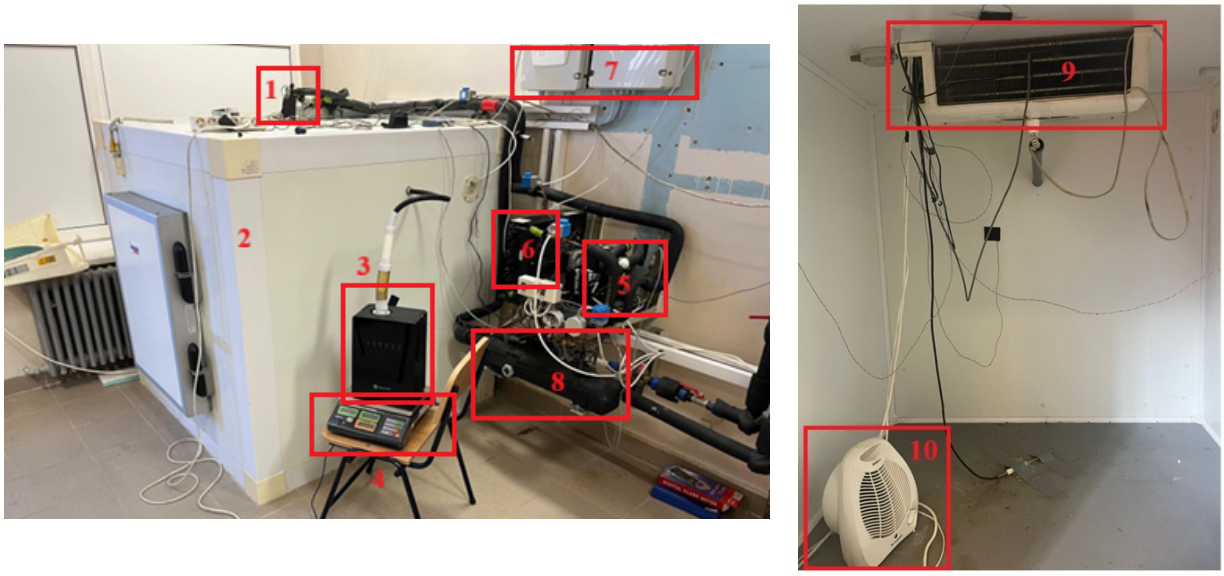
The paper is structured as follows: Section 2 presents materials and methods focusing on the experimental setup, the model of the PCM-based defrosting system, uncertainty analysis and validation. Section 3 presents the results and discussion, while Section 4 highlights the main conclusions.

2. Materials and Methods

2.1. Experimental Setup

The experimental setup described in this section was used to experimentally establish the amount of ice that can be supported by the given refrigeration system. This amount of ice would later be used in the model of the PCM-based defrosting system.

An overview image of the experimental setup is given in Figure 1. Basically, the experimental setup comprises a 1.7 m^3 cold room equipped with a VCRS operating with refrigerant R404A. The rated cooling capacity of the VCRS is roughly 1500 W.



(**a**) (**b**)

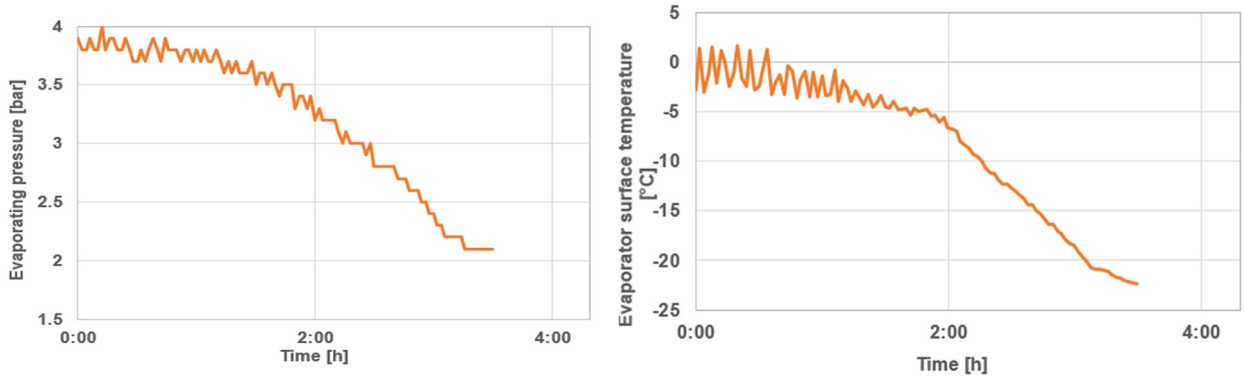
Figure 1. Experimental setup image: (**a**) Exterior view and (**b**) view inside the cold room. 1—Expansion valve; 2—Cold room; 3—Vapor generator; 4—Weight measurement device (scale); 5—Compressor; 6—Condenser; 7—Data acquisition system; 8—Liquid tank; 9—Evaporator; 10—Heat source.

To simulate the thermal load of the refrigeration system, a controlled electric heater (Figure 1b index 10) was used. The purpose was to maintain a median 4 °C air temperature inside the cold room by intermittent operation between 3 °C and 5 °C. Therefore, continuous operation of the refrigeration system was ensured. For simulating the humidity load, a vapor generator was used. The relative humidity inside the cold room was not recorded. The vapor generator was manually controlled to ensure a continuous water vapor flow, providing a constant latent cooling load with the primary objective of forcing frost accumulation on the evaporator over the cooling operation mode. A negligible amount of the water vapor condensed at the contact with the cold room walls, and the rest was found as ice on the evaporator. In the experimental setup from Figure 1, the defrost was carried out using the EHD, incorporating an electrical heater at 460 W. The PCM-DS was not installed on the experimental setup, but the VCRS was used to collect data to design it. Using the vapor generator and a scale, it was observed that in 3.5 h, the evaporator of the VCRS accumulated approximately 1 kg of ice, meaning a vapor generation rate of 0.08 g/s. The experimental setup was fitted with temperature sensors and pressure transducers. A temperature sensor and a pressure transducer were mounted at the exit of the evaporator.

Figure 2 shows the ice layer formed on the evaporator after 3.5 h of operation. One can notice an uneven distribution of the ice layer and severe obstruction of the airflow path. The air velocity at the exit of the evaporator was not recorded. Figure 3a shows that the evaporating pressure drops from 3.9 bar to 2.1 bar, and consequently, the evaporating temperature drops from roughly −13 °C to −30 °C during the 3.5 h of operation. As the evaporating temperature drops, so does the temperature of the evaporator coil, as shown in Figure 3b. At the end of the 3.5 h of operation, the superheating temperature of the refrigerant drops significantly from −3.3 °C to −21.6 °C, as seen in Figure 4.



Figure 2. Evaporator covered with 1 kg of ice.



(**a**) (**b**)

Figure 3. (**a**) Evaporating pressure over time for 1 kg of formed ice and (**b**) evaporator surface temperature.

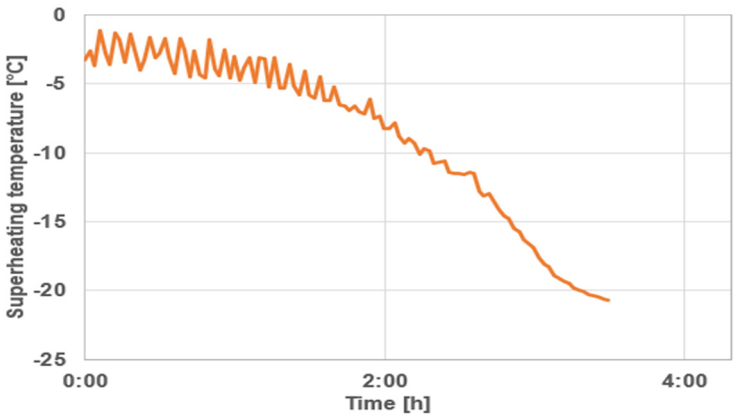


Figure 4. Superheating temperature over time for 1 kg of formed ice.

In the next section, the model for the PCM-based defrosting system (PCM-DS) is presented.

2.2. Model of the PCM-Based Defrosting System

The model of the PCM-DS is developed considering Figures 5 and 6.

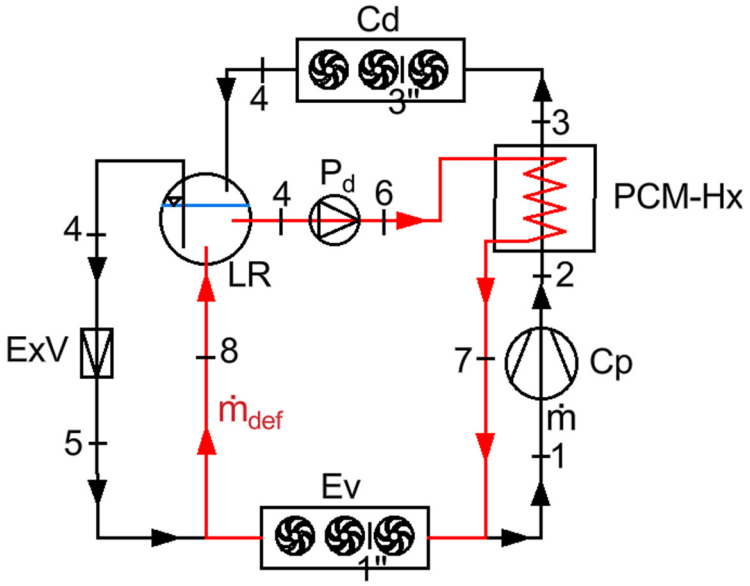


Figure 5. Schematic of VCRS with PCM-DS.

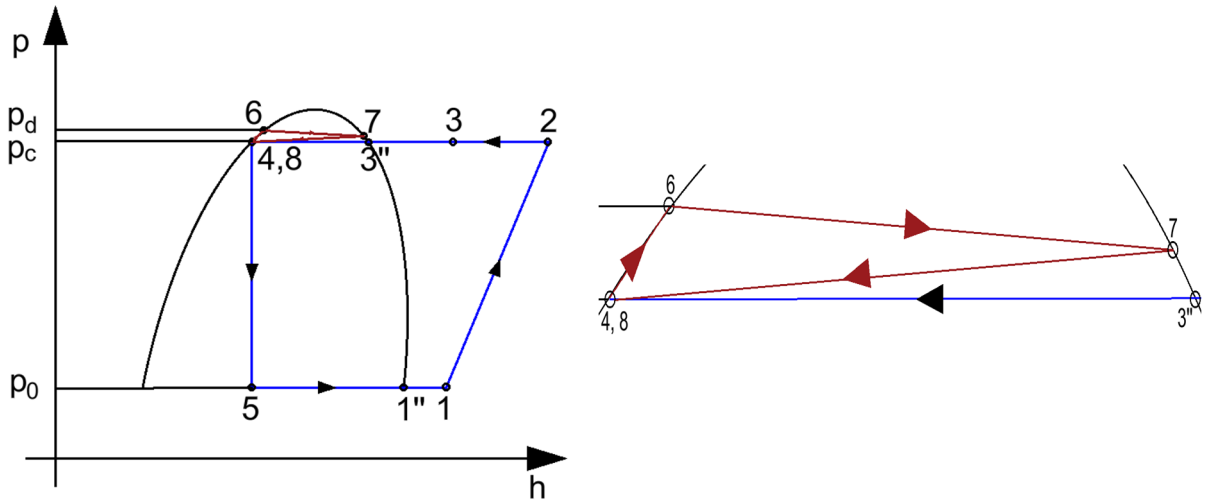


Figure 6. Cycle of VCRS with PCM-DS.

Figure 5 shows the simplified schematic of the given VCRS together with the PCM-DS. The operation of the VCRS is presented in correlation with Figure 6, which shows the corresponding thermodynamic cycle. The VCRS can operate in two modes: (i) cooling operating mode (COM) and (ii) defrosting operating mode (DOM). In COM, the refrigerant passes through the VCRS, following the path marked with a black line in Figure 5, and it undergoes the well-known corresponding thermodynamic processes, as shown in Figure 6. The energy corresponding to process 2–3 is stored by the PCM in the phase change material heat exchanger (PCM-Hx from Figure 5). In DOM, the VCRS stops, and the pump (Pd from Figure 5) is turned on. The refrigerant follows the path marked with a red line in Figure 5. In the PCM-Hx, at the beginning of DOM, the PCM is in a liquid state due to the energy absorbed in the desuperheating process (2–3 from Figure 6) during COM. In the PCM-Hx, the refrigerant evaporates (process 6–7 from Figure 6), and in the Ev, it condensates and

transfers heat to the formed ice (7–8 from Figure 6). With state 8, the liquid refrigerant enters the LR, and the process is resumed. The Pd is a circulation pump, and it covers only the pressure losses on the refrigerant flow path. These pressure losses have been assumed at a value of 0.6 bar to account for the circulation pump power input in the present study. Figure 6 shows the thermodynamic cycle of the VCRS along with the PCM-DS operation.

The model of the PCM-DS was developed considering the assumptions presented in Table 1.

Table 1. Assumptions.

Operating Mode		Assumptions
COM	1	The operation of the VCRS is in steady state.
	2	The compression process is isentropic.
	3	The internal and external irreversibility sources at the VCRS level are neglected.
	4	The minimum temperature of the ice formed on the evaporator is assumed to be equal to the saturation temperature corresponding to the evaporating pressure at the end of the 3.5 h of operation.
	5	The condensing temperature is considered constant and unaffected by the PCM transient temperature variations.
	6	The temperature of the refrigerant in state 3 is equal to the PCM melting temperature.
	7	The maximum temperature of the liquid PCM is 4 °C higher than its melting temperature during COM of the VCRS, when the energy from the desuperheating process (2–3) is used.
DOM	8	The refrigerant in the PCM-Hx in state 7, from Figure 6, is in a saturated vapor state.
	9	The refrigerant in state 8, from Figure 6, is in a saturated liquid state in the evaporator.
COM and DOM	10	The ambient temperature surrounding the VCRS is 23 °C.
	11	The heat loss to the environment in the PCM-Hx is not neglected.
	12	The phase change temperature of the PCM is considered constant along the process, representing the mean integral value of the melting range.

For the thermodynamic cycle, the compression process was considered to be a theoretical one (isentropic) because the experimental setup did not allow for the evaluation of the isentropic efficiency of the compressor (assumption 1 according to Table 1). Regarding the condensing temperature, it was set to a constant value because the condensing pressure during the operation of the experimental setup ranged between 17.4 and 18.1 bar. Also, the pressure drop in the condenser was neglected (assumption 5 according to Table 1). For DOM, the refrigerant entered the PCM-Hx as a saturated liquid (state 6 from Figure 5), and it was assumed that at exit (state 7 from Figure 5), it was in a dry, saturated vapor state. With state 7, the refrigerant entered the evaporator, where it would melt the ice, and consequently, it would completely condensate to the thermodynamic state 8, a saturated liquid. These assumptions (8 and 9 from Table 1) were made considering the scenario of melting 1 kg of ice. If the mass of ice changes and the refrigerant mass flow rate is constant, the thermodynamic state 8 would also change. The constant phase change temperature of the PCM (assumption 12 from Table 1) was considered based on the PCM data sheet.

The mathematical model in the present work is approached considering steady-state operation and the energy balance equations for both COM and DOM. The work intends to estimate the mass of PCM, the mass flow rate of refrigerant, energy consumption during DOM and the theoretical COP of the VCRS with and without PCM-DS and EHD. These results will show if such a system is feasible. Such preliminary work is justified by the lack

of papers dealing with this subject in the literature. The main limitations of applying the steady-state modeling of the present system are related to the inherently transient heat transfer and phase-change phenomena that occur during COM and DOM at the PCM-Hx level. The model is developed considering an imposed defrosting period. If the transient heat transfer mechanisms are taken into consideration, it is highly probable that the values given by the steady-state modeling are consistently different from the transient heat transfer case. During DOM, the boundary between liquid and solid PCM moves as the defrost time decreases, meaning that the liquid fraction is decreasing and the solid fraction is increasing. Also, some PCMs like OM42, OM46 and OM48 are organic mixtures, meaning that they do not have a constant temperature during phase change. Nevertheless, steady-state modeling can be used as a preliminary assessment tool of the practical benefit of such a defrosting system. Based on the energy balance equations, a preliminary mass of PCM, refrigerant mass flow rate during DOM, and the energy consumption of such PCM-DS can be evaluated. If the steady-state modeling based on energy balances shows that the proposed PCM-DS has reasonable dimensions compared to the dimensions of the VCRS presented in Figure 1, it is worth moving to more complicated mathematical modeling involving transient heat transfer, PCM phase change behavior, natural convective currents that occur in the liquid superheated PCM and other transient phenomena. The ultimate goal would be to design the PCM-DS, especially the PCM-Hx, as accurate as possible in order to achieve defrosting in a given time period.

If the system proves feasible, future work will be conducted in order to approach the heat transfer mechanisms, the finite volume method, and experimental work, to better estimate the behavior of the PCM-DS. Differences between the current work and future work involving heat transfer mechanisms, the finite volume method, and the experimental work are expected.

The PCM-DS is intended to be mounted on the experimental setup presented in Section 2.1. In order to do so, the PCM-DS has to be designed. Next, a steady-state model that describes the operation of the PCM-DS is developed, aiming to find the mass of PCM and the defrosting refrigerant mass flow rate.

Step 1—Characterization of the VCRS in COM

From the operation of the experimental setup presented in Figure 1, the evaporating and condensing pressures can be derived along with the amount of ice formed on the evaporator. These values are presented in Table 2 for the moment when the VCRS starts and after 3.5 h of operation.

Table 2. Parameters of the VCRS.

	Parameter	**Symbol**	**Value**
Start of the VCRS	Evaporating pressure	p_0	3.9 bar
	Condensing pressure	p_c	18 bar
	Mass of ice	m_{ice}	0 g
End of 3.5 h of operation	Evaporating pressure	p_0	2.1 bar
	Condensing pressure	p_c	17.4 bar
	Mass of ice	m_{ice}	1 kg

Based on the data presented in Table 2, a program in the Engineering Equation Solver V10.836-3D [24] was developed, allowing for the determination of the temperature, enthalpy, entropy, specific volume and quality in the characteristic points 1″, 1, 2, 3, 3″, 4, 5, 6, 7, 8 (see Figure 6). The program also includes Equations (1)–(8). The governing

Equations (1)–(41) applied in the present mathematical model represent the fundamental steady-state thermodynamic and heat transfer energy balances according to [25–27].

The cooling capacity of the VCRS is:

$$\dot{Q}_0 = \dot{m} \cdot (h_1 - h_5) \quad (1)$$

The theoretical mechanical power of the compressor is:

$$P_{cp} = \dot{m} \cdot (h_2 - h_1) \quad (2)$$

Using Equations (1) and (2), the theoretical coefficient of performance can be evaluated:

$$COP = \dot{Q}_0 / P_{cp} \quad (3)$$

The refrigerant mass flow rate in COM, $\dot{m}$ can be estimated using the constructive characteristics of the compressor as:

$$\dot{m} = \dot{V}_1 / v_1 \quad (4)$$

The volume flow rate of the compressor $\dot{V}_1$ is:

$$\dot{V}_1 = \lambda \cdot \dot{V}_s \quad (5)$$

The specific volume v_1 from Equation (4) corresponds to state 1 from Figure 6.

The flow rate coefficient λ can be computed as:

$$\lambda = 1 - \varepsilon_0 \cdot ((p_c / p_0)^{(1/n)} - 1) \quad (6)$$

The theoretical flow rate $\dot{V}_s$ of the compressor is:

$$\dot{V}_s = V_s \cdot (nr/60) \quad (7)$$

The displacement V_s of the compressor is:

$$V_s = \frac{\pi \cdot D^2}{4} \cdot S \cdot i \quad (8)$$

The characteristics of the compressor needed to compute Equations (1)–(8) are presented in Table 3 and have been obtained by dismounting and measuring an identical compressor.

Table 3. Compressor characteristics.

	Symbol	Value	Units
Diameter	D	0.0349	m
Stroke	S	0.0192	m
Compressor speed	n_r	3000	rot min^{-1}
Dead space volume coefficient	ε_0	0.025	-
Number of cylinders	i	1	-
Polytropic index	n	1.1	-
Refrigerant		R404A	

Step 2—Establishing the heat rate needed to melt the ice formed on the evaporator

The heat rate $\dot{Q}_{ice}$ required to melt m_{ice} is:

$$\dot{Q}_{ice} = (Q_s + Q_l)/\tau_{def} \quad (9)$$

$$Q_s = m_{ice} \cdot c_{ice} \cdot (0 - t_{ice}) \quad (10)$$

$$Q_l = m_{ice} \cdot q_{ice} \quad (11)$$

Step 3—Estimating the PCM mass needed to ensure the heat rate demand to melt the ice formed on the evaporator

The mass of PCM, m_{PCM}, required to absorb the heat rate needed to melt the ice $\dot{Q}_{ice}$ can be determined as follows:

$$(Q_{s\ SH} + Q_f + Q_{s\ SC})/t_{def} - \dot{Q}_{walls} = \dot{Q}_{ice} \quad (12)$$

$$Q_{s\ SH} = m_{PCM} \cdot c_{PCM\ liquid} \cdot (t_{SH} - t_{PC}) \quad (13)$$

$$Q_f = m_{PCM} \cdot q_{PC} \quad (14)$$

$$Q_{s\ SC} = m_{PCM} \cdot c_{PCM\ solid} \cdot (t_{PC} - t_c) \quad (15)$$

Step 4—Finding the refrigerant mass flow rate that can ensure ice melting in DOM

The refrigerant mass flow $\dot{m}_{def}$ required to absorb the energy stored in the PCM during COM, which is released on the formed ice on the evaporator in DOM, can be determined from:

$$\dot{Q}_{ice} = (Q_{s\ SH} + Q_f + Q_{s\ SC})/\tau_{def} - \dot{Q}_{Walls} = \dot{m}_{def} \cdot (h_7 - h_6) \quad (16)$$

The defrosting refrigerant mass flow rate can also be expressed as:

$$\dot{m}_{def} = \dot{Q}_{ice}/(h_7 - h_8) \quad (17)$$

Equations (9)–(17) correspond to the design stage of the PCM-DS, having the main focus on finding the mass of PCM and the refrigerant mass flow rate in DOM.

Next, the work focuses on pointing out the behavior of the PCM-DS in other conditions of operation.

Energy balance equations for PCM-Hx and VCRS cooling operating mode

Heating stage

$$(m_{PCM} \cdot c_{PCM\ solid} \cdot (t_{PC} - t_{SC}))/\tau_{SC-PC} = \dot{m} \cdot (h_2 - h_3) - \dot{Q}_{walls} \quad (18)$$

Phase change stage

$$(m_{PCM} \cdot q_{PC})/\tau_{melting} = \dot{m} \cdot (h_2 - h_3) - \dot{Q}_{walls} \quad (19)$$

The superheating stage

$$(m_{PCM} \cdot c_{PCM\ liquid} \cdot (t_{SH} - t_{PC}))/\tau_{PC-SH} = \dot{m} \cdot (h_2 - h_3) - \dot{Q}_{walls} \quad (20)$$

Energy balance equations for PCM-Hx and VCRS defrosting operating mode

Cooling stage

$$(m_{PCM} \cdot c_{PCM\ liquid} \cdot (t_{SH} - t_{PC}))/\tau_{SH-PC} - \dot{Q}_{Walls} = \dot{m}_{def} \cdot (h_7 - h_6) \quad (21)$$

Phase change stage

$$(m_{PCM} \cdot q_{PC}) / \tau_{solidifyng} - \dot{Q}_{walls} = \dot{m}_{def} \cdot (h_7 - h_6) \quad (22)$$

Subcooling stage

$$(m_{PCM} \cdot c_{PCM\ solid} \cdot (t_{PC} - t_c)) / \tau_{PC-SC} - \dot{Q}_{Walls} = \dot{m}_{def} \cdot (h_7 - h_6) \quad (23)$$

The heat rate lost to the surroundings $\dot{Q}_{walls}$ was computed by the authors, considering a free convection heat transfer application [28]. The mathematical model to compute $\dot{Q}_{walls}$ is presented below for a L × W × H (0.15 m × 0.15 m × 0.15 m) cubic PCM-Hx:

$$\dot{Q}_{walls} = \frac{\alpha_{air} \cdot \left(t_{pcm,sh} - t_{amb}\right) \cdot A_{walls}}{1000} \quad (24)$$

where $A_{walls} = \left(6 \cdot L^2\right)$ and represents the total area of heat transfer.

The heat transfer coefficient α_{air} can be computed as follows:

$$\alpha_{air} = \frac{Nu_m \cdot \lambda_{air}}{L} \quad (25)$$

where Nu_m is the Nusselt number and can be expressed as:

$$Nu_m = C_{con} \cdot (Gr \cdot Pr)^{n_{con}} \quad (26)$$

where C_{con}= 0.135 and $n_{con} = 0.33$ based on $Gr \cdot Pr$ criteria.

The Grashof criteria can be expressed as:

$$Gr = \frac{\beta_{air} \cdot 9.81 \cdot L^3 \cdot \left(t_{pcm,sh} - t_{amb}\right)}{{\nu_{air}}^2} \quad (27)$$

The Prandtl criteria can be expressed as:

$$Pr = \frac{\nu_{air}}{a_{air}} \quad (28)$$

Ambient air properties such as β_{air} (coefficient of volumetric thermal expansion), a_{air} (thermal diffusivity), λ_{air} (thermal conductivity) and ν_{air} (kinematic viscosity) were computed using EES software (V10.836-3D) in conditions of 1 bar atmospheric pressure and 23 °C ambient temperature.

The theoretical COP of the VCRS without the PCM-DS can be computed according to Equation (3).

The theoretical COP of the VCRS with the PCM-DS is:

$$COP_{def} = (\dot{Q}_0 \cdot \tau_{cooling}) / (P_{cp} \cdot \tau_{cooling} + P_{def} \cdot \tau_{def}) \quad (29)$$

If the DOM is carried out using an electric heater, as is the case for the one mounted on the experimental setup, the theoretical COP can be computed:

$$COP_{def} = (\dot{Q}_0 \cdot \tau_{cooling}) / (P_{cp} \cdot \tau_{cooling} + P_{res} \cdot \tau_{def}) \quad (30)$$

where P_{res} is the power input of the electrical resistance of the EHD.

$$\tau_{cooling} = \tau_{total} - \tau_{def} \quad (31)$$

The power of the circulation pump P_d of the PCM-DS is:

$$P_{def} = \dot{m}_{def} \cdot (\Delta p \cdot 10^5) / \rho_{liquid\ ref} \quad (32)$$

where $\rho_{liquid\ ref}$ is the density of the liquid refrigerant in state 6 from Figure 6, and Δp represents the pressure losses that are covered by the circulation pump.

The energy consumption E_{def} of the circulation pump P_d is:

$$E_{def} = P_{def} \cdot \tau_{def} \quad (33)$$

Exposure of PCM to multiple phase change cycles can lead to the degradation of the thermophysical properties, such as thermal conductivity and latent heat [29], and exposure to extreme temperatures can lead to mass losses [30]. Based on these, the authors have proposed an energy storage management strategy for the PCM inside the PCM-Hx during COM of the VCRS. From the authors' knowledge, this energy storage management strategy has not been examined in the literature. The authors propose three energy storage management strategies that will be explained with numerical examples in Section 3.

Strategy 1—Unique superheating. This strategy involves heating the PCM from the PCM-Hx since the start of COM. The PCM goes through the three stages: heating, phase change and superheating, which result in t_{SH}. Next, using the energy available from the desuperheating process (2–3 from Figure 6), the PCM is kept at constant t_{SH} for a time $\tau_{superheating}$ until COM ends and DOM starts.

$$\tau_{superheating} = \tau_{total} - \tau_{def} - \tau_{melting} \quad (34)$$

Strategy 2—Unique bypass. This strategy involves a process wherein, after the previous defrosting process, the refrigerant discharged by the compressor is bypassed directly to the condenser. As a consequence, the PCM from the PCM-Hx is cooled under the influence of the surrounding air temperature. Its temperature decreases from t_c to t_{amb} and remains constant for a certain period of time. Next, based on a controller, the refrigerant discharged by the compressor is directed to the PCM-Hx, and thus the PCM is heated, melted and superheated in such a way that, at the end of the COM, its temperature is t_{SH}.

Subcooling time from t_c to t_{amb} can be found from:

$$(m_{PCM} \cdot c_{PCM\ solid} \cdot (t_c - t_{amb})) / \tau_{c-amb} = \dot{Q}_{Walls} \quad (35)$$

Time while the PCM temperature is equal to t_{amb}:

$$\tau_{equilibrum} = \tau_{total} - \tau_{def} - \tau_{melting} \ - \ \tau_{c-amb} - \tau_{amb-c} \quad (36)$$

Heating time from t_{amb} to t_c can be determined from:

$$(m_{PCM} \cdot c_{PCM\ solid} \cdot (t_c - t_{amb})) / \tau_{amb-c} = \dot{m}_{def} \cdot (h_2 - h_3) - \dot{Q}_{Walls} \quad (37)$$

Time required for heating from t_c to t_{SH} can be found as follows:

$$(m_{PCM} \cdot c_{PCM\ solid} \cdot (t_{PC} - t_c) + m_{PCM} \cdot q_{PC} + m_{PCM} \cdot c_{PCM\ liquid} \cdot (t_{SH} - t_{PC})) / \tau_{melting} = \dot{m} \cdot (h_2 - h_3) - \dot{Q}_{Walls} \quad (38)$$

Strategy 3—Intermittent bypass. This strategy involves heating the PCM from the PCM-Hx since the start of COM. The PCM goes through the three stages: heating, phase change and superheating, resulting in, at the end of the superheating process, t_{SH}. Next, based on a controller, the PCM from the PCM-Hx suffers intermittent connections from the discharge of the compressor to the PCM-Hx, which leads to temperature fluctuations of the

PCM from t_{PC} to t_{SH} until DOM is activated. The temperature of PCM decreases from t_{SH} to t_{PC} because of $\dot{Q}_{Walls}$ influence.

The time for the 3 stages of heating of the PCM after the previous DOM can be expressed as:

$$(m_{PCM}\cdot c_{PCM\ solid}\cdot(t_{PC}-t_c)+m_{PCM}\cdot q_{PC}+m_{PCM}\cdot c_{PCM\ liquid}\cdot(t_{SH}-t_{PC}))/\tau_{melting}\ =\dot{m}\cdot(h_2-h_3)-\dot{Q}_{Walls} \quad (39)$$

Cooling time from t_{SH} to t_{PC}:

$$(m_{PCM}\cdot c_{PCM\ liquid}\cdot(t_{SH}-t_{PC}))/\tau_{SH-PC}\ =\dot{Q}_{walls} \quad (40)$$

Superheating time from t_{PC} to t_{SH}:

$$(m_{PCM}\cdot c_{PCM\ liquid}\cdot(t_{SH}-t_{PC}))/\tau_{PC-SH}=\dot{m}\cdot(h_2-h_3)-\dot{Q}_{Walls} \quad (41)$$

The schematic of the unique and intermittent energy storage management strategy can be seen in Figure 7. The red line follows DOM and the black line follows for COM of the VCRS while the grey line follows for the bypass path.

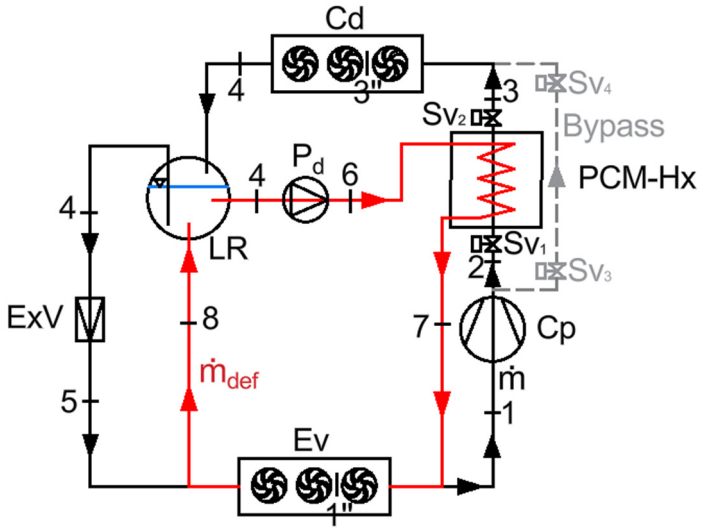


Figure 7. Schematic of the VCRS with PCM-DS for the unique and intermittent bypass energy storage management strategy.

2.3. Uncertainty Analysis

The uncertainty corresponding to the quantities computed in the present work can be determined with the following equation, according to [31]:

$$u_y=\sqrt{\left(\frac{\partial y}{\partial x_1}\cdot u_{x_1}\right)^2+\left(\frac{\partial y}{\partial x_2}\cdot u_{x_2}\right)^2+\ldots\ldots+\left(\frac{\partial y}{\partial x_n}\cdot u_{x_n}\right)^2} \quad (42)$$

In Equation (42), x_1 to x_n represent the independent variables (measured experimental parameters, such as pressure, temperature and mass of ice) and y is the dependent variable. u_{x1} to u_{xn} are the absolute uncertainties associated with each independent variable.

Table 4 presents the type of sensors used to measure the experimental parameters and their associated absolute uncertainty. Using Engineering Equation Solver, an uncertainty propagation analysis was conducted based on the data from Table 4. The absolute uncertainties for the measured parameters have a marginal influence on the compressor parameters, pressure drop, and thermodynamic properties of the refrigerant, having a less than 1% relative uncertainty. The measured parameters do not influence the PCM

properties or the heat loss coefficient. The latter are based on the theoretical assumptions mentioned in Table 1.

Table 4. Type of sensors and absolute uncertainty.

Measured Parameters	Type of Sensors	Range	Absolute Uncertainty
Superheating temperature t_1	NTC	−50/105 °C	±1 °C
Evaporating pressure p_0	Pressure transducer	−0.5/7 bar	±0.075 bar F.S.
Condensing pressure p_c	Pressure transducer	0/30 bar	±0.3 bar F.S.
Mass of ice	Scale	0/15 kg	±0.005 kg

Table 5 shows the influence of experimental instruments and absolute and relative uncertainties of main calculated data.

Table 5. Influence of experimental instruments and uncertainties of main calculated data.

Dependent Variable	Value	Absolute Uncertainty ±	Relative Uncertainty %	Independent Variable			
				m_{ice}	p_0	p_c	t_1
m_{PCM} OM42	2.118 kg	0.0099 kg	0.46	x			
m_{PCM} OM46	2.315 kg	0.0107 kg	0.46	x			
m_{PCM} OM48	2.504 kg	0.0114 kg	0.45	x			
$\dot{m}_{def}$ **10^{-3}**	1.768 kg s^{-1}	0.0174 kg s^{-1}	0.98	x		x	
h_6	380.4 kJ kg^{-1}	0.11 kJ kg^{-1}	0.028			x	
h_7	259 kJ kg^{-1}	1.14 kJ kg^{-1}	0.44			x	
E_{def}	197.4 W h	2.68 W h	1.35	x		x	
COP	3.31	0.098	2.97		x	x	
COP_{def}	3.21	0.096	3	x	x	x	x
τ_{SC-PC}	97.92 s	26 s	26.5	x	x	x	x
$\tau_{melting}$	1632 s	162.2 s	9.9	x	x	x	x
τ_{PC-SH}	104.6 s	11.17 s	10.6	x	x	x	x
τ_{SH-PC}	102.6 s	$1.1 \cdot 10^{-11}$ s	$1.07 \cdot 10^{-11}$	x	x	x	x
$\tau_{solidifyng}$	1601 s	17.2 s	1.07			x	
τ_{PC-SC}	96.4 s	17.2 s	17.89			x	
$\tau_{superheating}$	10,766 s	195.9 s	1.8	x	x	x	x
τ_{c-amb}	6464 s	268.6 s	4.15	x		x	
$\tau_{equilibrum}$	3877 s	206.5 s	5.3	x	x	x	x
τ_{amb-c}	424.6 s	35 s	8.2	x	x	x	x
τ_{bypass}	1592 s	7.44 s	0.46	x			

Note: The marker "x" shows which independent variable is used to compute the dependent variable.

The uncertainty associated with the results presented is very small. As a consequence, for clarity over the figures presented, the uncertainties are presented numerically in the comments corresponding to the figures from Section 3.

2.4. Validation

Due to the lack of literature dealing with PCM-DS for refrigeration systems that is unrelated to heat pumps, it is difficult to find related work. As such, the results given by the current steady-state model in terms of PCM mass are compared to [17], which deals with a PCM-DS for an 8.9 kW heat pump. The authors investigated a PCM-DS based on 35% mollauric acid and 65% molcapric acid, using the heat available on the compressor shell during the operation of the heat pump. For melting approximately 1 kg of ice, the authors reported a mass of 4.2 kg of PCM. Out of this mass, the authors stated that only 80% was actually used in the defrosting process, meaning an effective mass of 3.42 kg of PCM. Considering that the PCM used has the latent heat of fusion of 133 kJ/kg and the OM42 proposed in the current paper has one of 190 kJ/kg, this leads to an equivalent mass of 2.3 kg of OM42 that would have been used in the application reported by [17] to melt the same amount of ice. This value is very close to the value estimated by the steady-state model of 2.1 kg, with an 8% difference. This means that the estimation of the OM42 mass obtained by the steady-state model is feasible. In another work, ref. [19] reported a mass of 3.1 kg of Calcium Chloride Hexahydrate used for defrosting a 2.5 kW air heat pump system. Out of this, the authors reported that only 50% of the PCM was actually used in the defrosting process for 0.35 kg of ice. It seems that there is a tendency to over-size the PCM-Hx in terms of thermal storage. One possible explanation for oversizing is the complicated nature of heat transfer mechanisms, the convective currents that occur during the phase-change processes and other energy losses.

In the next section, the advantages and disadvantages of the three strategies will be discussed.

3. Results and Discussions

Based on the equations presented in Section 2.2, a program has been developed in Engineering Equation Solver [24].

The three PCM candidates presented in Table 6 have been chosen, among many others reported in the literature, because of their melting temperature suitable for the operating conditions of the present VCRS. The melting temperature is lower than the discharge temperature (t_2 from Figure 6) and higher than the condensing temperature (t_c from Figure 6). At the same time, these PCM candidates are easily available on the market and are financially accessible.

Table 6. Properties of three PCM candidates.

Property	Symbol	OM42	OM46	OM48
Melting temperature	$t_{melting}$ [°C]	44	47	51
Solidifying temperature	$t_{solidifying}$ [°C]	43	45	48
Latent heat	q [kJ kg^{-1}]	194.5	178	168.5
Solid specific heat	c_{solid} [kJ kg^{-1} K^{-1}]	2.71	2.5	2.02
Liquid specific heat	c_{liquid} [kJ kg^{-1} K^{-1}]	2.78	2.7	2.35
Density, solid	ρ_{solid} [kg m^{-3}]	903	917	960
Density, liquid	ρ_{liquid} [kg m^{-3}]	863	880	875
Thermal conductivity, solid	k_{solid} [W m^{-1} K^{-1}]	0.19	0.2	0.2
Thermal conductivity, liquid	k_{liquid} [W m^{-1} K^{-1}]	0.1	0.1	0.1
Flammability	200 °C	Yes	No	Yes

Figure 8 presents the masses of PCM for OM42, OM46 and OM48, respectively. The results presented are obtained using: p_0 = 3.9 bar, $\dot{Q}_{walls} = 15\ W$ and t_{def} = 1800 s. One can notice that the smallest mass of PCM is obtained for OM42, followed by OM46 and OM48. In Figure 8, it can be seen that the mass of OM42 is 10% lower than that of OM46 and roughly 20% lower than that of OM48. The mass of PCM is influenced by the m_{ice} measured with the scale. This influence resulted in roughly ±0.46% for OM42, ±0.46% for OM46 and ±0.45% for OM48, regarding RU for the mass of PCM. In these conditions, the PCM chosen for the present study is OM42. The main reasons are the lowest phase change temperature, mass and volume of the PCM-Hx. Also, it could be used in other operation conditions of the VCRS. Although this chosen PCM ignites at 200 °C, in the present case, it is out of the danger zone because the discharge temperature is considerably lower, even if a real compression process (not the ideal one approached in the paper) is considered. The results that follow are generated considering OM42.

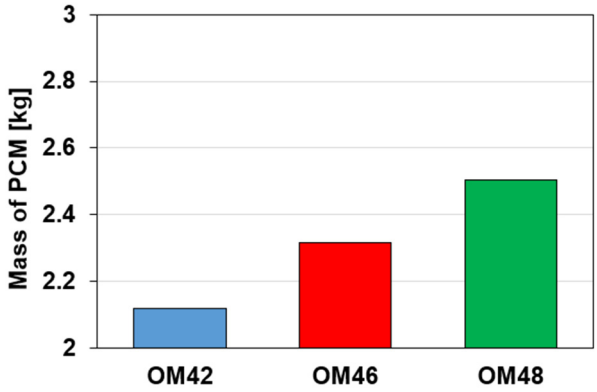


Figure 8. Mass of the PCM candidates.

Figure 9 shows the mass flow rate of refrigerant in DOM over ice quantity. Figure 9 was generated considering the following conditions: p_0 = 3.9 bar, p_c = 18 bar and t_{def} = 1800 s. Also, the refrigerant enters the evaporator in saturated vapor state 7 from Figure 6 and exits the evaporator in saturated liquid state 8 from Figure 6. As can be seen, the m_{ice} formed on the evaporator increases, so does the $\dot{m}_{def}$ needed to melt it during DOM of the VCRS. For 1 kg of ice, $\dot{m}_{def} = 0.001768$ kg/s. The RU associated with $\dot{m}_{def}$ is ±0.98%, and it is mainly influenced by the uncertainty of m_{ice} along with p_c.

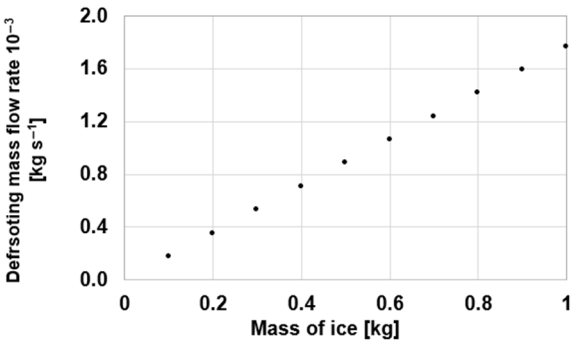


Figure 9. Mass flow rate of refrigerant in defrosting mode over ice quantity.

Figure 10 highlights the energy consumed by the defrost circulation pump during DOM in two situations: variable t_{def} with constant $\dot{m}_{def}$ and constant t_{def} with variable $\dot{m}_{def}$.

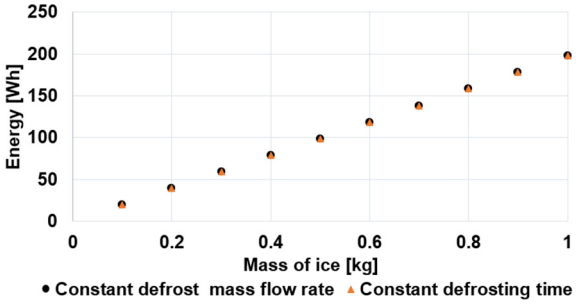


Figure 10. Energy consumption of the defrost circulation pump.

In Figure 10, one can notice that as m_{ice} increases, so does E_{def}. The results presented in Figure 10 are obtained considering: p_0 = 3.9 bar, p_c = 18 bar and t_{def} = 1800 s. Also, in this case, the refrigerant enters the evaporator in saturated vapor state 7 from Figure 6 and exits the evaporator in saturated liquid state 8 from Figure 6, for t_{def} = ct. In the case of $\dot{m}_{def} = ct$, the results presented are obtained using p_0 = 3.9 bar and $\dot{m}_{def}$ = 0.001768 kg/s. It can be observed that E_{def} has the same values in the two situations analyzed. This behavior is a consequence of the evolution of t_{def} and the evolution of $\dot{m}_{def}$, as shown in Figure 9. More exactly, if m_{ice} increases, the necessary $\dot{m}_{def}$ increases by the same amount as the decrease in t_{def}. It is noticeable that, in practice, the situation preferred by the user would be choosing a lower t_{def} for the same E_{def}. The RU associated with E_{def} is ±1.35% due to the uncertainty of m_{ice} and p_c.

In Figure 11, one can notice that the theoretical COP of the VCRS without PCM-DS is constant over the increase in m_{ice} because no additional energy consumption is required other than the energy needed for the compressor in COM. The results presented correspond to the unique superheating energy storage management strategy. Figure 11 is obtained in the following conditions: p_0 = 3.9 bar, p_c = 18 bar and superheating temperature t_1 = −3.3 °C for both COPs compared. Additionally, in the case of the COP of the VCRS with DS, the conditions are completed with: $t_{cooling}$ = ct and $\dot{m}_{def}$ = 0.001768 kg/s. If the VCRS is equipped with a PCM-DS, additional energy consumption is required for the operation of P_d, the same as in the EHD case for the operation of the P_{res}. This additional energy increases as the m_{ice} increases and, in consequence, the COP decreases. For 1 kg of defrosted ice, the COP of the VCRS is roughly 3% higher than the COP of the VCRS with PCM-DS and 5.6% higher than the COP of the VCRS with EHD. This is an optimistic result as it does not account for valve losses, added pressure drop, control system losses, extra refrigerant charge, and heat-transfer limitations. These penalties will be considered in future work and will be determined for the real-size experimental setup. Because the PCM-DS is not installed on the experimental setup, and this work is a steady-state feasibility analysis, these values have not been considered. In an ideal case, the power of the electric heater should be equal to the heat rate needed for melting 1 kg of ice in 30 min. This yields a power of 0.21 kW. From the steady-state model, to melt the same amount of ice with the current PCM-DS, the power needed for the operation of P_d is 109 W. The difference between the two methods is 48%. This considerable difference will be reflected in the COP value. For the ideal EHD, the COP yields 2.85, while for PCM-DS, it is 2.93, meaning a 2.70% higher value in the case of PCM-DS for 1 kg of ice defrosted.

This proves the theoretical feasibility of the proposed PCM-DS. The COP is expected to be lower if heat transfer mechanisms are considered for the PCM-DS and not only the energy balance equations. The COP of the VCRS is influenced by p_0 and p_c and accounts for ±2.97% RU, while the COP of the VCRS with PCM-DS is influenced by all independent variables involving a ±3% RU.

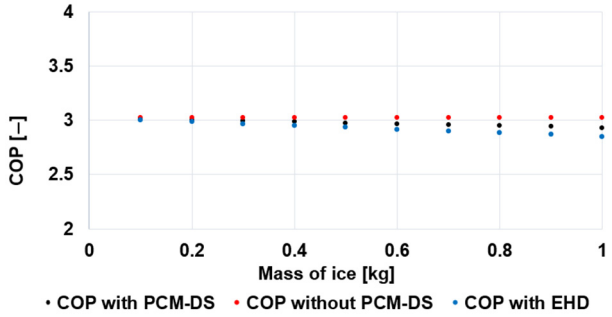


Figure 11. Theoretical COP of the VCRS with and without PCM-DS and EHD.

The next group of results elaborates on the three energy storage management strategies presented at the end of Section 3. The time periods presented are generated using $\dot{m}_{def} = 0.001768$ kg/s in DOM and using $\dot{m} = 0.01548$ kg/s in COM.

Figure 12 shows the evolution of the temperature of the PCM during one defrosting cycle and one cooling cycle of the VCRS. The vertical line that can be seen at exact 14,400 s represents the end of both COM and DOM, after 4 h of operation. The start of the analysis of Figure 12 is time 0, when the defrosting cycle begins. The defrost is enabled for 1800 s during which the PCM is cooled ($102.6 \pm 1.1 \times 10^{-11}$ s), solidifies (1601 ± 17.2 s) and subcools (96.4 ± 17.2 s). After 1800 s, the COM is enabled for 12,600 s during which the PCM is heated (97.92 ± 26 s), melts (1632 ± 162.2 s) and is superheated (104.6 ± 11.17 s). After the PCM reaches its superheated state, it stays in this state until the next DOM is enabled ($10{,}766 \pm 195.9$ s). This strategy assures that, at the end of COM, the PCM has a superheated state that ensures the necessary energy storage to melt 1 kg of ice. In terms of operation, for this management strategy, no additional solenoid valves and automation systems are required. The refrigerant flows right through the PCM-Hx. The main advantage of this method is that the VCRS does not suffer any changes compared to the schematic shown in Figure 5.

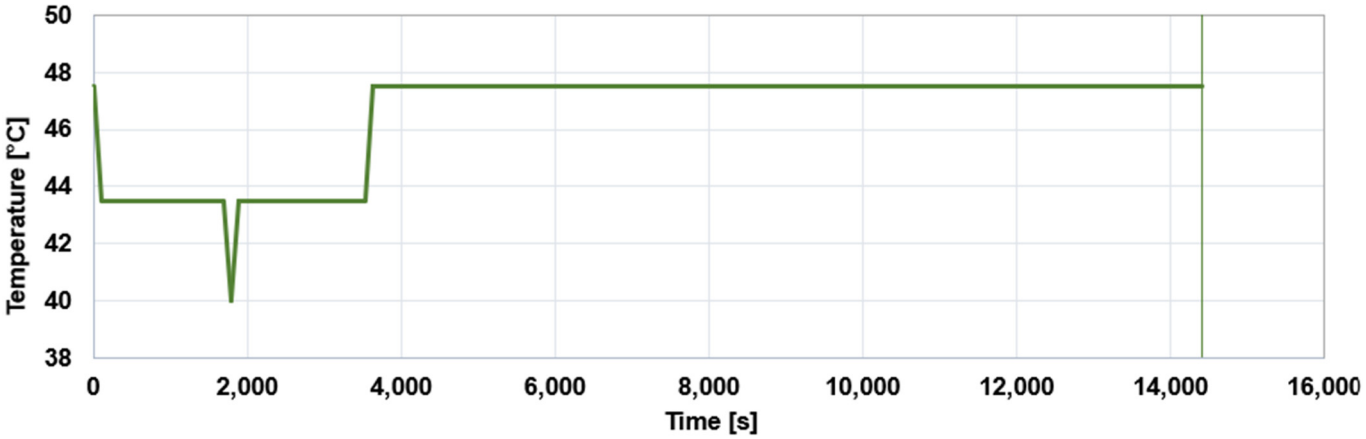


Figure 12. Unique superheating energy storage management strategy. Temperature of the PCM for a complete COM and DOM cycle.

Figure 13 emphasizes the behavior of the PCM during one defrosting cycle and one cooling cycle of the VCRS for the unique bypass energy storage management strategy. The vertical line that can be seen at exact 14,400 s represents the end of both COM and DOM, after 4 h of operation. The defrost is enabled for 1800 s, the same as in Figure 12. At this time, the discharged refrigerant from the compressor is directed to the condenser via a bypass, and no refrigerant passes through the PCM-Hx, as shown in Figure 7. Next, the cooling operation cycle is enabled. During this cycle, the PCM from the PCM-Hx cools

due to the heat exchange with the surroundings for 6464 ± 268.6 s until it reaches t_{amb} and remains at this temperature (assumption to simplify the model) for 3877 ± 206.5 s, until a controller deactivates the bypass and the refrigerant discharged by the compressor flows through the PCM-Hx. The controller operates in such a way that the moment of deactivating the bypass is determined by estimating the time needed to heat (522 ± 61 s), melt (1632 ± 162.2 s) and superheat (104.6 ± 11.17 s) the mass of PCM in order to have enough energy stored to melt 1 kg of ice. This time can be estimated through the current work under theoretical conditions. After DOM is finished, SV3 and SV4 are opened, and SV1 and SV2 are closed. With 2258 s before another DOM cycle, SV3 AND SV4 are closed, and SV1 and SV2 are open. The main advantage of this energy storage management strategy is that, at the end of COM, the PCM is in a superheated state that can ensure the melting of the ice formed on the evaporator. The main disadvantage is that the schematic from Figure 5 would accommodate the bypass system, as presented in Figure 7.

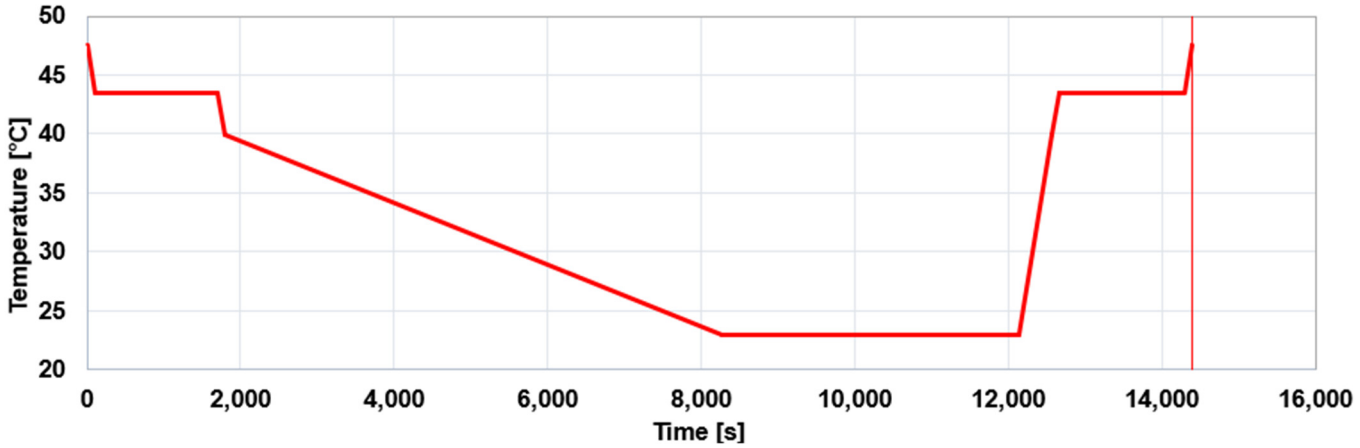


Figure 13. Unique bypass energy storage management strategy. Temperature of the PCM for a complete COM and DOM cycle.

In Figure 14, one can notice the intermittent bypass energy storage management strategy of the PCM during one defrosting cycle and one cooling cycle of the VCRS. The vertical line that can be seen at exact 14,400 s represents the end of both COM and DOM, after 4 h of operation. The defrost is enabled for 1800 s, the same as in Figures 12 and 13. After COM is enabled, the PCM from the PCM-Hx is heated (97.92 ± 26 s), melted (1632 ± 162.2 s) and superheated (104.6 ± 11.17 s) under the influence of the discharged refrigerant by the compressor. During this cycle, once the temperature of the PCM reaches the t_{SH}, a controller deactivates the bypass, and the refrigerant no longer flows through the PCM-Hx. Thus, the PCM will start to cool due to heat exchange with the surroundings for 1592 ± 7.4 s seconds until it reaches the solidification temperature. At this moment in time, the bypass is activated, and the refrigerant discharged by the compressor flows once more through the PCM-Hx for 104.6 ± l11.17 s. This process of activating and deactivating the bypass continues until DOM is enabled. For the present study, there are seven intermittent bypass cycles. This energy storage management strategy could be applied in cases where there are high discharge temperatures, and according to [30], the long exposure to extreme temperatures can lead to the degradation of the thermophysical properties of the PCM. One of the main disadvantages of this strategy is accommodating the bypass system, as seen in Figure 7. Also, as seen in Figure 14, at the end of COM, the temperature of the PCM might be lower compared to the previously used energy storage management strategy. The temperature of the PCM is roughly 46 °C due to the operation of the bypass energy storage process, which did not fully occur because DOM is enabled. Having PCM from

PCM-Hx with a lower temperature than the superheated temperature, the system might not be able to defrost 1 kg of ice. At the end of DOM, SV1 and SV2 are open, while SV3 and SV4 are closed. The PCM will be heated, melted and superheated. At this moment, the intermittent bypass management strategy is activated, meaning intermittent engages of SV1 and SV2 (SV3 and SV4 are closed) and intermittent engages of SV3 and SV4 (SV1 and SV2 are closed), totaling a number of 28 engages.

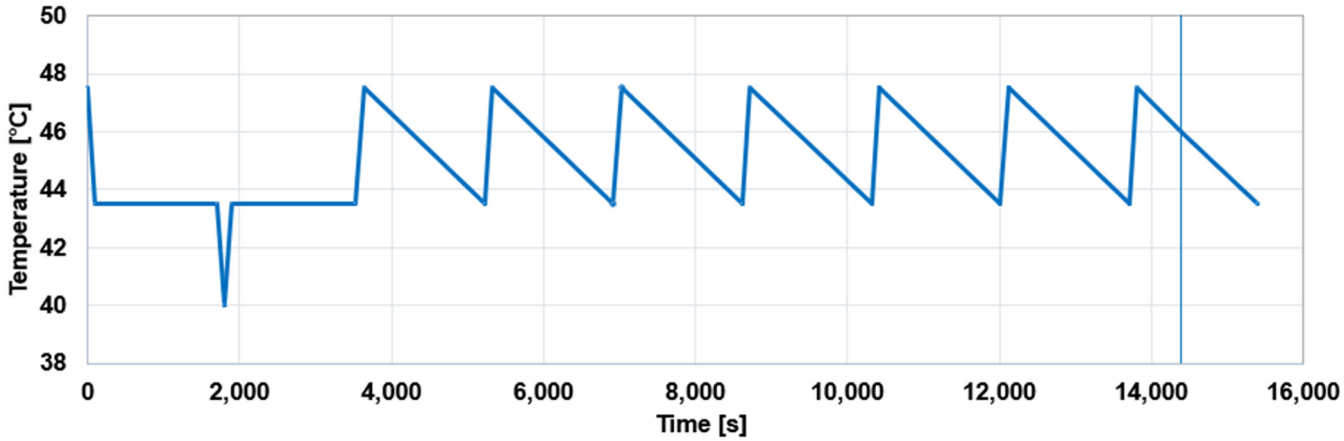


Figure 14. Intermittent bypass energy storage management strategy. Temperature of the PCM for a complete COM and DOM cycle.

The energetic performance of the three energy storage management strategies is expected to be in the following relationship: unique superheating has the lowest energy consumption, followed by the unique bypass and the intermittent bypass energy storage management strategies. The energy consumption for the three strategies is estimated based on the number of solenoid valves needed for the bypass. In the proposed strategies, the unique superheating requires no energy penalty for solenoid valves. Next, the unique bypass generates additional energy consumption for the four solenoid valves, while the intermittent bypass requires the activation of four solenoid valves more frequently.

From the three energy storage management strategies presented above, the authors would recommend the unique superheating energy storage management strategy because it has the highest COP, the lowest number of melting and solidification cycles and additional modification to the VCRS is not required. If the degradation of the thermophysical properties of the PCM is of interest, according to [29], there is a limited number of cycles (complete phase change from liquid to solid and vice versa) to which the PCM can be subjected, roughly 2000. In the present work, for 3.5 h of operation and 0.5 h of defrosting, 24 h per day, 2000 cycles yield 167 days of operation for all three management strategies. Theoretically, if the findings from reference [29] are applied, PCM from the PCM-Hx should be replaced after 167 days in the conditions of the present study. This is a subject for further investigation of the PCM-DS. This value should not be seen as a confirmed replacement time.

In Table 7, the three management strategies are compared in terms of the final temperature of the PCM at the start of DOM, the number of melting and solidification cycles, additional automation system, the number of solenoid valves, the number of engages of the solenoid valves, the estimated power demand, the solenoid valves' energy consumption and the theoretical COP of the system. One can notice that, in the case of the intermittent bypass management strategy, the final temperature of the PCM at the start of DOM is less than 47.5 °C, which is required for the defrosting process of 1 kg of ice. The highest number of solidification and melting cycles is requested for the intermittent bypass management strategy, followed by the unique superheating and unique bypass management strategies.

In the case of the unique bypass and the intermittent bypass management strategies, an additional automation system capable of monitoring and identifying the right moment for opening and closing the solenoid valves is required. The minimum number of solenoid valves required is zero for the unique superheating management strategy and four for the unique bypass and intermittent bypass management strategy. The number of solenoid valves engaged is proportional to the number of melting and solidification cycles, having the highest value of 28 for intermittent bypass, followed by 4 valves engaged for unique bypass, and no engages for the unique superheating management strategy. In terms of power demand, the lowest value is recorded for the unique superheating (0 W), followed by the unique bypass (40 W), and the intermittent bypass (280 W). The energy consumption is proportional to the number of solenoid valves engaged and the operation time corresponding to each melting and solidification cycle. The highest energy consumption is obtained for the intermittent bypass management strategy (272 kJ), because it has the highest number of engages and the highest operation time. The energy consumption for the solenoid valves of the three management strategies also has to be integrated into the value of the theoretical COP of the VCRS with PCM-DS, using Equation (24). As can be seen, the highest COP is obtained for unique superheating (2.93), followed by unique bypass (2.82) and intermittent bypass (2.81).

Table 7. Comparison between the three management strategies.

Management Strategy	PCM Temperature * [°C]	Number of Melting (m) and Solidification (s) Cycles	Additional Automation Equipment	Number of Solenoid Valves	Number of Engages	Estimated Power Demand [W]	Solenoid Valves Energy Consumption [kJ]	COP_{tot}
Unique superheating	47.5	1 m	no	0	0	0	0	2.931
Unique bypass	47.5	1 m	yes	4	4: 1 × SV1 + 1 × SV2 + 1 × SV3 + 1 × SV4	40	252	2.824
Intermittent bypass	46	7 m + 7 s	yes	4	14: 7 × SV1 + 7 × SV2 + 7 × SV3 + 7 × SV4	280	272	2.816

* Final temperature of the PCM at the start of DOM.

4. Conclusions

The present work proposes a phase change material-based defrosting system for vapor compression refrigeration systems. A steady-state macroscopic thermodynamic model, governed by global energy balances and driven by experimental boundary conditions, evaluates the VCRS in both cooling and defrosting operating modes. Among the three candidates investigated (OM42, OM46, OM48), OM42 was selected for minimizing system mass and volume constraints. The key findings are as follows: In terms of energy consumption, EHD requires 48% more energy than PCM-DS for defrosting. This leads to a 5.6% (EHD) and 3% (PCM-DS) penalty compared to the theoretical COP of the VCRS. For the ideal EHD, the COP yields 2.85, while for PCM-DS, it is 2.93, meaning a 2.7% higher value in the case of PCM-DS for 1 kg of ice defrosted. Three distinct energy storage management strategies were evaluated: unique superheating, unique bypass, and intermittent bypass. The results show that the highest COP is obtained for unique superheating (2.93), followed by unique bypass (2.82) and intermittent bypass (2.81). Using the intermittent bypass management strategy leads to an insufficient thermal load to defrost 1 kg of ice, as a consequence of the PCM temperature (46 °C) at the end of the cooling operating mode. The number of solenoid valves engaged is proportional to the number of melting and solidification cycles. The minimum number of solenoid valves required is 0 for the unique superheating management strategy. The work conducted proves a theoretical feasibility for such PCM-DS combined with a unique superheating management strategy. The limitations

in the present work include not considering the transient heat transfer mechanisms and the lack of experimental data to realistically evaluate the pressure drops, isentropic efficiencies, control system losses, extra refrigerant charge and valve losses. Future work will focus on developing the mathematical model considering transient heat transfer mechanisms; variable phase change temperature of the phase change processes; variable thermal conductivity, depending on liquid/solid fractions; variable specific heat during the phase change interval; and also the geometry of the heat transfer surface area corresponding to the phase change material-based heat exchanger.

Author Contributions: Conceptualization, A.C. and H.P.; Methodology, A.C. and H.P.; Software, A.C., C.I. and V.A.; Validation, D.T. and V.A.; Formal analysis, A.C.; Investigation, H.P.; Resources, V.A. and H.P.; Data curation, C.I. and D.T.; Writing—original draft preparation, A.C. and H.P.; writing—review and editing, C.I. and D.T.; Visualization, H.P. and C.I.; supervision, V.A.; Project administration, V.A.; Funding acquisition, C.I. All authors have read and agreed to the published version of the manuscript.

Funding: The APC was funded by the Romanian Ministry of Education and Research and the National University of Science and Technology POLITEHNICA Bucharest through the PubArt program.

Data Availability Statement: The original contributions presented in the study are included in the article.

Acknowledgments: The authors would like to acknowledge the Research Center in Mechanical Engineering and Mechatronics, Faculty of Mechanical Engineering and Mechatronics from National University of Science and Technology POLITEHNICA Bucharest, for providing the experimental infrastructure used in the present study.

Conflicts of Interest: The authors declare no conflicts of interest.

Abbreviations

The following abbreviations are used in this manuscript:

c	specific heat [kJ kg^{-1} K^{-1}]
D	diameter [m]
E	energy [W h]
g	gravitational acceleration [m s^{-2}]
h	specific enthalpy [kJ kg^{-1}]
i	number of cylinders [-]
k	thermal conductivity [W m^{-1} K^{-1}]
m	mass [kg]
$\dot{m}$	refrigerant mass flow rate [kg s^{-1}]
n	politropic index [-]
n_r	compressor speed [rot min^{-1}]
p	pressure [bar]
P	power input [W]
Q	heat [kJ]
$\dot{Q}$	heat rate [kW]
S	stroke [m]
t	temperature [°C]
v	specific volume [m^3 kg^{-1}]
x	vapor quality [-]
Cd	condenser
COP	coefficient of performance
COM	cooling operating mode
Cp	compressor
DOM	defrosting operating mode

EES	Engineering Equation Solver
EHD	electric heating defrost
Ev	evaporator
ExV	expansion valve
F.S.	full scale
HVAC&R	heating, ventilation, air conditioning, and refrigeration
LR	liquid receiver
NTC	negative temperature coefficient
PCM	phase change material
PCM-Hx	phase change material heat exchanger
PCM-DS	phase change material-based defrosting system
P_d	defrost circulation pump
P_{res}	electrical-resistance power input
RU	relative uncertainty
SV	solenoid valve
TES	thermal energy storage
VCRS	vapor compression refrigeration system
Δ	increment
ε_0	dead-space volume coefficient [-]
λ	flow rate coefficient [-]
ρ	density [kg m^{-3}]
τ	time [s]
0	evaporating
1	superheating
2	discharging
amb	ambient
c	condensing
cp	compressor
def	defrost
ice	ice
l	latent
liquid	liquid state
PC	phase change
SC	subcooled
SH	superheated
ref	refrigerant
res	resistance
s	sensible
solid	solid state
walls	walls

References

1. Hepbasli, A. Low Exergy (LowEx) Heating and Cooling Systems for Sustainable Buildings and Societies. *Renew. Sustain. Energy Rev.* **2012**, *16*, 73–104. [CrossRef]
2. Amer, M.; Wang, C.-C. Review of Defrosting Methods. *Renew. Sustain. Energy Rev.* **2017**, *73*, 53–74. [CrossRef]
3. Awate, G.D.; Acharya, A.; Kulkarni, A. Review on Defrosting Methods for Heat Pump When Outdoor Coil Surface Temperature Falls Below Zero-Degree Temperature. *Int. J. Eng. Sci. (TIJES)* **2020**, *7*, 56–59.
4. Bansal, P.; Fothergill, D.; Fernandes, R. Thermal Analysis of the Defrost Cycle in a Domestic Freezer. *Int. J. Refrig.* **2010**, *33*, 589–599. [CrossRef]
5. Hoffenbecker, N.; Klein, S.A.; Reindl, D.T. Hot Gas Defrost Model Development and Validation. *Int. J. Refrig.* **2005**, *28*, 605–615. [CrossRef]
6. Song, M.; Xia, L.; Deng, S. A Modeling Study on Alleviating Uneven Defrosting for a Vertical Three-Circuit Outdoor Coil in an Air Source Heat Pump Unit During Reverse Cycle Defrosting. *Appl. Energy* **2016**, *161*, 268–278. [CrossRef]

7. Abdel-Wahed, R.M.; Hifni, M.A.; Sherif, S.A. Hot Water Defrosting of a Horizontal Flat Plate Cooling Surface. *Int. J. Refrig.* **1983**, *6*, 152–154. [CrossRef]
8. Wu, X.M.; Webb, R.L. Investigation of the Possibility of Frost Release from a Cold Surface. *Exp. Therm. Fluid Sci.* **2001**, *24*, 151–156. [CrossRef]
9. Zhang, P.; Hrnjak, P.S. Air-Side Performance of a Parallel-Flow Parallel-Fin (PF2) Heat Exchanger in Sequential Frosting. *Int. J. Refrig.* **2010**, *33*, 1118–1128. [CrossRef]
10. Tan, H.; Xu, G.; Tao, T.; Sun, X.; Yao, W. Experimental Investigation on the Defrosting Performance of a Finned-Tube Evaporator Using Intermittent Ultrasonic Vibration. *Appl. Energy* **2015**, *158*, 220–232. [CrossRef]
11. Liang, X.; Wu, L. A Brief Review: The Mechanism; Simulation and Retardation of Frost on the Cold Plane and Evaporator Surface. *Energy Build.* **2022**, *272*, 112366. [CrossRef]
12. Song, M.; Deng, S.; Dang, C.; Mao, N.; Wang, Z. Review on Improvement for Air Source Heat Pump Units During Frosting and Defrosting. *Appl. Energy* **2018**, *211*, 1150–1170. [CrossRef]
13. Qu, M.; Li, T.; Deng, S.; Fan, Y.; Li, Z. Improving Defrosting Performance of Cascade Air Source Heat Pump Using Thermal Energy Storage Based Reverse Cycle Defrosting Method. *Appl. Therm. Eng.* **2017**, *121*, 728–736. [CrossRef]
14. Aljabair, S.; Alesbe, I.; Ibrahim, S.H. Review on Latent Thermal Energy Storage Using Phase Change Material. *J. Therm. Eng.* **2023**, *9*, 247–256. [CrossRef]
15. Chetan, T.; Pradip, R.S.; Thagamani, G.; Ramasamy, T. Phase Change Materials for Domestic Refrigerators to Improve Food Quality and Prolong Compressor off Time. In Proceedings of the International Refrigeration and Air Conditioning Conference, West Lafayette, IN, USA, 12–15 July 2010.
16. Li, Z.-L.; Zhang, C.-L.; Liu, H.-M.; Wang, X.-C. Feasibility Analysis of Thermal Storage Defrosting Method for Air Source Heat Pump: From Energetic and Economic Viewpoints. *Appl. Therm. Eng.* **2024**, *236*, 121828. [CrossRef]
17. Long, Z.; Dong, J.; Jiang, Y.; Yao, Y. A Novel Defrosting Method Using Heat Energy Dissipated by the Compressor of an Air Source Heat Pump. *Appl. Energy* **2014**, *133*, 101–111. [CrossRef]
18. Liu, Z.; Zhao, F.; Zhang, L.; Zhang, R.; Yuan, M.; Chi, Y. Performance of Bypass Cycle Defrosting System Using Compressor Casing Thermal Storage for Air-Cooled Household Refrigerators. *Appl. Therm. Eng.* **2018**, *130*, 1215–1223. [CrossRef]
19. Hu, W.; Jiang, Y.; Qu, M.; Ni, L.; Yao, Y.; Deng, S. An Experimental Study on the Operating Performance of a Novel Reverse-Cycle Hot Gas Defrosting Method for Air Source Heat Pumps. *Appl. Therm. Eng.* **2011**, *31*, 363–369. [CrossRef]
20. Dong, J.; Jiang, Y.; Deng, S.; Yao, Y.; Qu, M. Improving Reverse Cycle Defrosting Performance of Air Source Heat Pumps Using Thermal Storage-Based Refrigerant Sub-Cooling Energy. *Build. Serv. Eng. Res. Technol.* **2012**, *33*, 223–236. [CrossRef]
21. Agyenim, F.; Hewitt, N.; Eames, P.; Smyth, M. A Review of Materials, Heat Transfer and Phase Change Problem Formulation for Latent Heat Thermal Energy Storage Systems (LHTESS). *Renew. Sustain. Energy Rev.* **2010**, *14*, 615–628. [CrossRef]
22. Joybari, M.M.; Haghighat, F.; Sedigh, S.; Al-Abidi, A.A. Heat Transfer Enhancement Techniques for PCM Thermal Energy Storage Systems. *Renew. Sustain. Energy Rev.* **2015**, *51*, 622–640.
23. Pucci, C.; Vanna, F.; Moro, L. Numerical Study of Latent Heat Thermal Energy Storage Enhancement by Nano-PCM in Aluminum Foam. *Inventions* **2018**, *3*, 76. [CrossRef]
24. *Engineering Equation Solver*, version 10.836; 64-bit Academic Professional V10.836-3D; Faculty of Mechanical Engineering, University Politehnica of Bucharest: București, Romania, 2020.
25. Dinçer, İ.; Kanoglu, M. *Refrigeration Systems and Applications*; John Wiley & Sons: Hoboken, NJ, USA, 2010.
26. Moran, M.J.; Shapiro, H.N.; Boettner, D.D.; Bailey, M.B. *Fundamentals of Engineering Thermodynamics*; John Wiley & Sons: Hoboken, NJ, USA, 2010.
27. Marin, M.; Colda, I.; Damian, A. Energy Case Studies on a Heat-Pump System for a Non-Residential Building. *Univ. Politeh. Buchar. Sci. Bull. Ser. C* **2012**, *74*, 73–84.
28. Marinescu, M.; Baran, N.; Radcenco, V. *Termodinamica Tehnica*, 2nd ed.; Matrix ROM: Bucuresti, Romania, 1998.
29. Song, M.; Pun, W.M.; Swapnil, D.; Pan, D.; Ning, M. Thermal Stability of Organic Binary PCMs for Energy Storage. *Energy Procedia* **2017**, *142*, 3287–3294. [CrossRef]
30. Katish, M.; Allen, S.; Squires, A.; Ferrandiz-Mas, V. Thermal Stability of Organic Phase Change Materials (PCMs) by Accelerated Thermal Cycling Technique. *Thermochim. Acta* **2024**, *737*, 179771. [CrossRef]
31. Li, L.; Wang, Q.; Liu, K.; Xing, Z.; Chen, Y.; Yang, Y.; Tian, H.; Shu, G. Experimental Study of a Composite Control Method Balancing High-Efficient and High-Executable Control for a CO_2 Refrigeration System. *Int. J. Refrig.* **2025**, *178*, 461–478. [CrossRef]

Disclaimer/Publisher's Note: The statements, opinions and data contained in all publications are solely those of the individual author(s) and contributor(s) and not of MDPI and/or the editor(s). MDPI and/or the editor(s) disclaim responsibility for any injury to people or property resulting from any ideas, methods, instructions or products referred to in the content.